PUNCTATE VASCULAR EXPRESSION1 Is a Novel Maize Gene Required for Leaf Pattern Formation That Functions Downstream of the Trans-Acting Small Interfering RNA Pathway[1][C][W][OA]

Xiaolan Zhang[2,3], Ryan N. Douglas[2], Josh Strable[2], Michelle Lee, Brent Buckner, Diane Janick-Buckner, Patrick S. Schnable, Marja C.P. Timmermans, and Michael J. Scanlon*

Plant Biology Department, University of Georgia, Athens, Georgia 30602 (X.Z.); Department of Plant Biology, Cornell University, Ithaca, New York 14853 (R.N.D., J.S., M.L., M.J.S.); Division of Science, Truman State University, Kirksville, Missouri 63501 (B.B., D.J.-B.); Center for Plant Genomics, Iowa State University, Ames, Iowa 50011 (P.S.S.); and Cold Spring Harbor Laboratory, Cold Spring Harbor, New York 11724 (M.C.P.T.)

The maize (*Zea mays*) gene *RAGGED SEEDLING2-R* (*RGD2-R*) encodes an ARGONAUTE7-like protein required for the biogenesis of trans-acting small interfering RNA, which regulates the accumulation of *AUXIN RESPONSE FACTOR3A* transcripts in shoots. Although dorsiventral polarity is established in the narrow and cylindrical leaves of rgd2-R mutant plants, swapping of adaxial/abaxial epidermal identity occurs and suggests a model wherein RGD2 is required to coordinate dorsiventral and mediolateral patterning in maize leaves. Laser microdissection-microarray analyses of the rgd2-R mutant shoot apical meristem identified a novel gene, *PUNCTATE VASCULAR EXPRESSION1* (*PVE1*), that is down-regulated in rgd2-R mutant apices. Transcripts of *PVE1* provide an early molecular marker for vascular morphogenesis. Reverse genetic analyses suggest that PVE1 functions during vascular development and in mediolateral and dorsiventral patterning of maize leaves. Molecular genetic analyses of *PVE1* and of rgd2-R;pve1-M2 double mutants suggest a model wherein PVE1 functions downstream of RGD2 in a pathway that intersects and interacts with the trans-acting small interfering RNA pathway.

Leaves are produced sequentially and reiteratively from the shoot apical meristem (SAM), a specialized pluripotent pool of stem cells located at the summit of plant shoots. Maize (*Zea mays*) leaf development is initiated by recruitment of about 200 founder cells from the flank of the SAM, a process that is visualized by the down-regulation of KNOTTED1-like homeobox protein accumulation in the apex and a switch from an indeterminate to a determinate cell fate (Poethig, 1984; Smith et al., 1992; Jackson et al., 1994; Poethig and Szymkowiak, 1995). Subsequent leaf patterning occurs along the proximodistal (base-tip), mediolateral (midrib-margin), and dorsiventral (adaxial/top-abaxial/bottom) axes to establish a fully differentiated, three-dimensional leaf primordium. The interactive mechanisms whereby lateral organ development is coordinated along three axes of growth is a fundamental question in plant biology.

Maize leaves have distinct adaxial and abaxial tissue types and the leaves are flattened along the mediolateral axis to increase the surface area available for light capture and gas exchange. Several mutants have been characterized in Arabidopsis (*Arabidopsis thaliana*), *Antirrhinum majus*, and maize that harbor apolar radially symmetric leaves lacking either adaxial or abaxial tissue (Waites and Hudson, 1995; McConnel et al., 1998; Timmermans et al., 1998). Examination of these radial leaf mutants has led to a model whereby the juxtaposition of adaxial and abaxial tissue types is required for mediolateral leaf development. A notable exception is the maize mutant ragged seedling2 (rgd2), which can develop radially symmetric leaves that maintain adaxial and abaxial tissue types yet still fail to expand mediolaterally (Henderson et al., 2005).

RGD2 encodes an ARGONAUTE7 (AGO7)-like protein that is required for biogenesis of a transacting small interfering RNA termed trans-acting small interfering RNA (ta-siARF; Douglas et al., 2010). The production of ta-siARF is a plant-specific process that utilizes both microRNA and siRNA biogenesis components in a single pathway (Allen et al., 2005; Yoshikawa

[1] This work was supported by the National Science Foundation (grant nos. 032195, 0638770, and 0820610).

[2] These authors contributed equally to the article.

[3] Present address: Department of Vegetable Science, China Agricultural University, Beijing, China 100193.

* Corresponding author; e-mail mjs298@cornell.edu.

The author responsible for distribution of materials integral to the findings presented in this article in accordance with the policy described in the Instructions for Authors (www.plantphysiol.org) is: Michael J. Scanlon (mjs298@cornell.edu).

[C] Some figures in this article are displayed in color online but in black and white in the print edition.

[W] The online version of this article contains Web-only data.

[OA] Open Access articles can be viewed online without a subscription.

www.plantphysiol.org/cgi/doi/10.1104/pp.111.192419

et al., 2005). ta-siARF production begins with the cleavage of the nonprotein coding *TAS3* transcripts by an RNA-induced silencing complex (RISC) composed of miR390 and RGD2/AGO7 (Allen et al., 2005; Adenot et al., 2006; Fahlgren et al., 2006; Douglas et al., 2010). Rather than being degraded, as would happen to most transcripts cleaved by a RISC, the cleavage product is stabilized and converted into double-stranded RNA in a process that requires LEAFBLADELESS1 (LBL1)/SUPPRESSOR-OF-GENE-SILENCING3, and RNA-DEPENDANT RNA POLYMERASE6. The double-stranded RNA undergoes phased cleavage by DICER-LIKE4 to yield 21-nucleotide mature ta-siARFs (Allen et al., 2005; Yoshikawa et al., 2005; Nogueira et al., 2007).

In Arabidopsis, ta-siARF forms a RISC with AGO1 to target transcripts of *AUXIN RESPONSE FACTOR3* (*ARF3*)/*ETTIN* and *ARF4* for degradation (Peragine et al., 2004; Hunter et al., 2006; Nogueira et al., 2007; Montgomery et al., 2008). Although *ARF3A* and ta-siARF have been described as polarity determinants (Fahlgren et al., 2006; Nogueira et al., 2007), their specific roles in maize leaf development are unclear. In wild-type maize, *ARF3A* accumulates in abaxial regions of leaf primordia. Surprisingly, *ARF3A* still accumulates abaxially in rgd2 and lbl1 mutants, which are deficient in ta-siARF biosynthesis (Douglas et al., 2010). These findings suggest that *ARF3A* transcripts are polarized independent of the ta-siARF biogenesis pathway.

To identify genes functioning downstream of ta-siARF biogenesis pathway, a microarray hybridization analysis of SAM-enriched maize cDNAs was performed utilizing laser microdissected (LM) tissue to compare transcript accumulation in wild-type and rgd2-R mutant apices. A novel maize gene named *PUNCTATE VASCULAR EXPRESSION1* (*PVE1*) is down-regulated in rgd2-R apices and exhibits a unique transcript accumulation pattern in maize shoot apices. We verified the down-regulation of *PVE1* transcripts in rgd2 mutant leaf primordia by quantitative reverse transcription (qRT)-PCR and demonstrate that *PVE1* is also down-regulated by mutations in *LBL1*, which functions downstream of *RGD2* during ta-siARF biosynthesis. Reverse genetic analyses reveal that PVE1 is required for normal vascular development and dorsiventral patterning in maize leaves; qRT-PCR analyses of pve1 mutants contribute to a model wherein PVE1 functions in a separate pathway downstream of the ta-siARF biogenesis pathway.

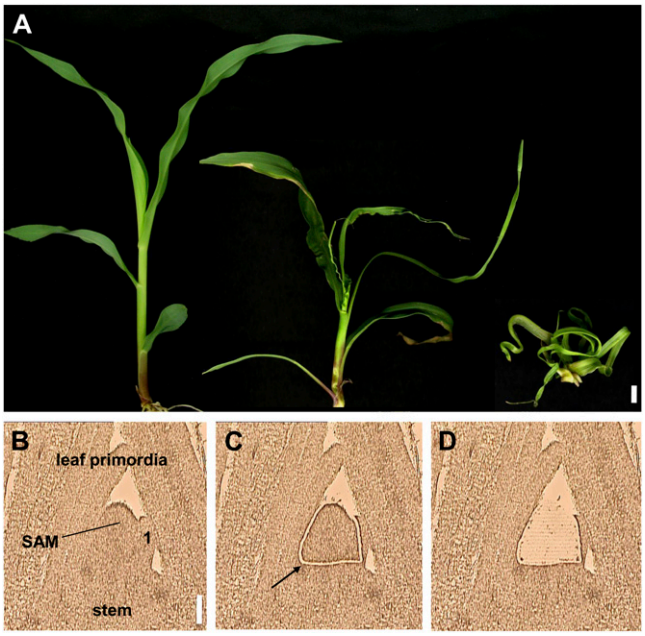

Figure 1. LM of the maize SAM cells from wild-type and rgd2-R mutants siblings. A, Leaf morphology of the rgd2-R mutant seedlings. Wild-type seedling (left) next to a phenotypically moderate (middle) and severe (right) rgd2-R mutant seedling. Bar = 1 cm. B to D, Light micrograph of a 10-μm longitudinal section of a maize shoot apex illustrates the LM of the SAM. Bar = 100 μm. B, SAMs before laser capture. C, Laser ablation cuts and destroys tissues surrounding the SAM, to isolate it from potentially contaminating stem and leaf tissues. D, SAM cells are removed by laser-pressure catapulting into collection caps suspended above the samples.

RESULTS

LM Microarray Analyses of the rgd2-R Mutant SAM

As reported previously (Henderson et al., 2005; Douglas et al., 2010), plants homozygous for the null mutation *rgd2-R* displayed a variable range of mutant shoot phenotypes (Fig. 1A). To identify downstream factors of the RGD2-mediated ta-siARF biogenesis pathway, especially genes that function during early stage of maize leave development, we performed meristem-specific transcriptome analyses using LM microarray. Maize SAM cells were harvested from 14-d-old rgd2-R mutant and wild-type seedlings by LM (Fig. 1). Six biological replicates were harvested, each comprising three to five whole SAMs from either mutant or wild-type plants; RNA extracted from the captured SAM cells was linearly amplified prior to its use in microarray hybridizations (Supplemental Table S1; "Materials and Methods"). Two maize gene arrays (SAM 1.1 and SAM 3.0 comprising 28,671 total elements and approximately 23,000 unique maize genes [described in Brooks et al., 2009]) were used in SAM-specific transcript profiling analyses. For each array platform, six biological replicates were hybridized with dye swapping to minimize dye-labeling bias. Data normalization and evidence test of differential expression were performed as described (Brooks et al., 2009).

A total of 178 genes were identified as differentially expressed in rgd2-R mutant SAMs, utilizing P value ≤ 0.001 or P values between 0.01 and 0.001 in combination with fold changes $\geq$2.0 (Supplemental Table S2). The average q value for this dataset is 0.44, a high false discovery rate that presumably results from the

extreme phenotypic variability observed in *rgd2-R* homozygous mutants. In light of this relatively high *q* value, the list of differentially expressed genes presented in Supplemental Table S2 is best utilized as a guide toward the selection of candidate genes for subsequent analyses and verification by qRT-PCR, in situ hybridization, and/or reverse genetic analyses, as demonstrated in the analysis of *PVE1* below.

PVE1 Is a Novel Gene Down-Regulated in the rgd2-R Mutant SAM

Among the 54 genes of unknown predicted function that were differentially expressed in the rgd2-R mutant shoot apex was the maize gene AC211276.4_FG008 (P = 0.00564, fold change = 0.18). qRT-PCR (Supplemental Table S4) verified the differential transcript accumulation of this gene (fold change = 0.16 ± 0.05), which was named *PVE1* based upon its distinct transcript accumulation pattern (Fig. 2). In situ hybridization analyses revealed that *PVE1* transcripts accumulate in an unusual punctate pattern, particularly over the vasculature in developing leaf primordia (Fig. 2). Longitudinal sections through the seedling SAM reveal *PVE1* transcript accumulation in intense foci, as well as diffuse spots of weaker transcript accumulation (Fig. 2A). Although the maize SAM and P1 leaf primordium are not yet vascularized, transverse sections through the shoot apex at the level of the leaf founder cells (Fig. 2B) reveal a punctate pattern of *PVE1* accumulation that precedes and predicts the eventual differentiation of vascular bundles in developing leaves. Accumulation of *PVE1* transcripts is dynamic within the vasculature of wild-type seedling shoots. Initially localized as a single spot within each developing vascular bundle of the young leaf primordia, *PVE1* transcripts later accumulate in at least two distinct spots per bundle corresponding to the fully differentiated phloem and xylem vessel elements of the P5 leaf primordium (Fig. 2C).

In agreement with our microarray and qRT-PCR data (Supplemental Tables S2 and S4), accumulation of *PVE1* transcripts is diminished in rgd2-R mutant SAMs, as indicated by fewer and smaller expression foci detected via in situ hybridizations (Fig. 2, D and E). Accumulation of *PVE1* transcripts remains diminished in rgd2-R mutant P1 and P2 leaf primordia, although spots of *PVE1* accumulation are detectable within the developing vasculature of the mutant P3 leaf (Fig. 2E). However in contrast to the pattern observed in wild-type vasculature, *PVE1* accumulation is consistently delayed within xylem vessels of rgd2-R mutants; in that mutant P5 leaf primordia exhibit *PVE1* accumulation in the phloem but not in the xylem (Fig. 2, E and F). In later-staged leaf primordia, *PVE1* transcripts are observed within both the phloem and xylem elements of rgd2-R mutants, a pattern that is comparable, albeit at lower transcript

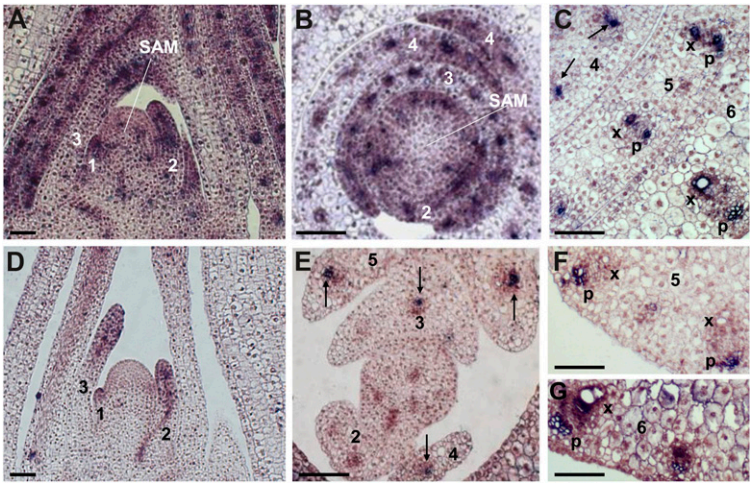

Figure 2. In situ hybridization analyses of *PVE1* transcript accumulation in the maize seedling shoot. Longitudinal (A) and transverse (B) sections of wild-type seedling apices reveal a punctate, interspersed accumulation pattern of *pve1* transcripts (purple-blue) over the vasculature, as well as in the SAM and P1 primordium prior to the development of vasculature. Gradients of *PVE1* expression are also noted between vascular bundles, in the leaf margins. C, Accumulation of *PVE1* transcript occurs in a single spot (arrows) in the undifferentiated vascular bundle of the wild-type P4 leaf (i.e. fourth leaf from the SAM), then separates into two discrete spots after differentiation of the xylem (x) and phloem (p) vascular components in the P5 and later leaves. D and E, Accumulation of *PVE1* transcript is greatly reduced in the rgd2-R mutant SAM and young leaf primordia. Note the aberrantly narrow leaf primordia observed in rgd2-R mutant seedlings. E, Expression is clearly detected in some developing vascular bundles of P3 mutant leaves and later (arrows in E). Although xylem and phloem vessels are well differentiated in P5 rgd2-R mutant leaves, *PVE1* accumulation appears normal in the phloem but is delayed in the xylem (F). At the P6 stage and later (G), *PVE1* accumulation in rgd2-R mutant leaves is similar to that in wild-type siblings. Numbers denote leaf primordia. Bars in A, B, D, and E = 50 μm; bars in C, F, and G = 25 μm.

abundance, to that observed in wild-type siblings (Fig. 2G). To corroborate the in situ hybridization data for leaf primordia, LM-qRT-PCR analyses of LM P1 to P4 leaf primordia revealed that in rgd2-R mutant leaves *PVE1* transcripts accumulate to 0.1- ± 0.2-fold the level detected in wild-type sibling leaves. Interestingly, *PVE1* accumulation decreased to 0.54- ± 0.08-fold the level of wild-type siblings in qRT-PCR analyses of lbl1-R mutant whole seedlings.

Found on maize chromosome 5 (http://www.maizesequence.org), the *PVE1* locus contains a single 3′ intron and generates a 1,513-bp transcript that comprises a 317-bp 5′-untranslated region (UTR), a single exon of 1,083 bp, and a 113-bp-long 3′-UTR that is predicted to encode a protein of 361 amino acids with no homology to proteins of known function (Fig. 3A; http://www.maizesequence.org). EST accession (EE186754) suggests that alternative transcripts may extend the 5′-UTR of *PVE1* to at least 763-bp upstream of the coding region (Fig. 3B), whereas a *PVE1* splicing variant fails to excise the 3′ intron and generates an extended 3′-UTR that is 535-bp long (Fig. 3C). Gene models for the predicted rice (*Oryza sativa*) ortholog of *PVE1* (LOC_Os03g44580) available at Gramene (http://www.gramene.org) reveal that equivalent transcript variants containing extended 5′-UTR sequences and/or unspliced 3′-UTR are also found in rice (Fig. 5D). In both maize and rice, neither the 3′-UTR nor the 5′-UTR extensions are predicted to further extend the open reading frame of the *PVE1* homologs.

Reverse Genetic Analyses of *PVE1* Function

Owing to its unusual expression profile and marked down-regulation in rgd2-R and lbl-R mutant shoots, a reverse genetic approach was utilized to investigate the function of PVE1 as a putative downstream component of the ta-siARF pathway. A PCR-based reverse genetic strategy exploiting the maize *Mutator* (*Mu*) transposon system (described in Brooks et al., 2009) utilized a combination of *PVE1*-specific and *Mu* transposon primers to identify two independent *Mu* transposon-insertion alleles of *PVE1*. Sequence analyses of plants homozygous for the *pve1-R* allele were found to contain a *Mu1*-like element inserted at base pair 614 of the coding region of *PVE1* (Fig. 3A), and a *Mu8*-like transposon insertion at base pair 280 gene cosegregates in plants containing the *pve1-M2* allele. Both of the independently derived *pve1* mutations contain transposon insertions within the lone exon of *PVE1*, and are predicted to be null alleles. In agreement with these predictions, RT-PCR utilizing primers spanning the *Mu* insertions in the *pve1-R* and *pve-M2* mutant alleles failed to amplify products from cDNA-derived pve1 mutant seedlings.

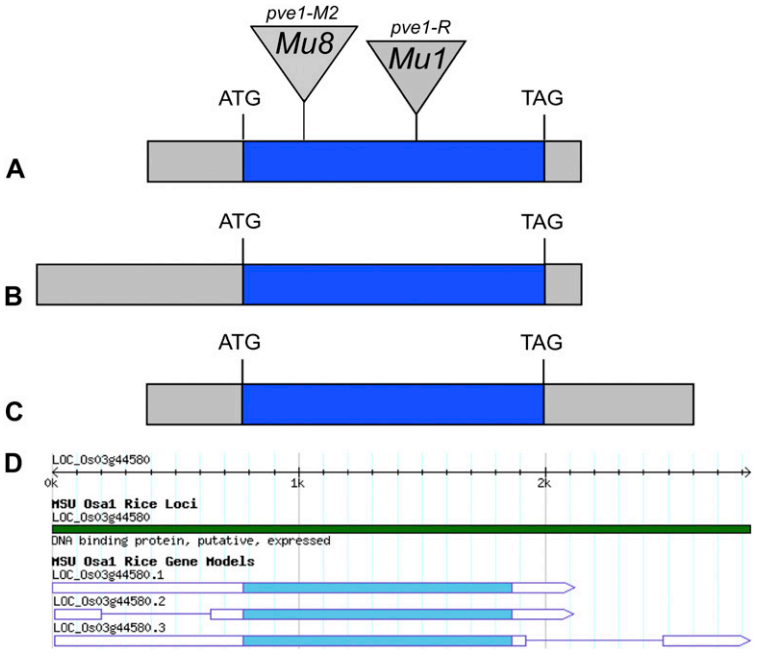

Figure 3. Structure of *PVE1* transcripts and alleles. A, *PVE1* has a 317-bp 5′-UTR (gray box) followed by a single 1,083-bp exon (blue box). A single intron is present in the 3′-UTR; following splicing the 3′-UTR is 113-bp long (gray box). The *pve1-R* mutation contains a *Mu1*-like (*Mu1*) element inserted at 614 bp of the coding region; the *pve1-M2* allele contains a *Mu8*-like insertion at bp 280. B, An EST (accession EE186754) suggests that the 5′-UTR of *PVE1* may extend at least 763-bp upstream of the coding region. C, One splice variant of *pve1* does not excise an intron in the 3′-UTR, resulting in a 3′-UTR that is 535-bp long. D, Rice gene models for LOC_Os03g44580, the closest rice homolog to *PVE1*, indicate that rice *PVE1*-like transcripts may also exhibit extended 5′-UTR sequences and an unspliced intron in the 3′-UTR as observed in maize. Image from: http://rice.plantbiology.msu.edu/cgi-bin/ORF_infopage.cgi?orf=3103.m04799. [See online article for color version of this figure.]

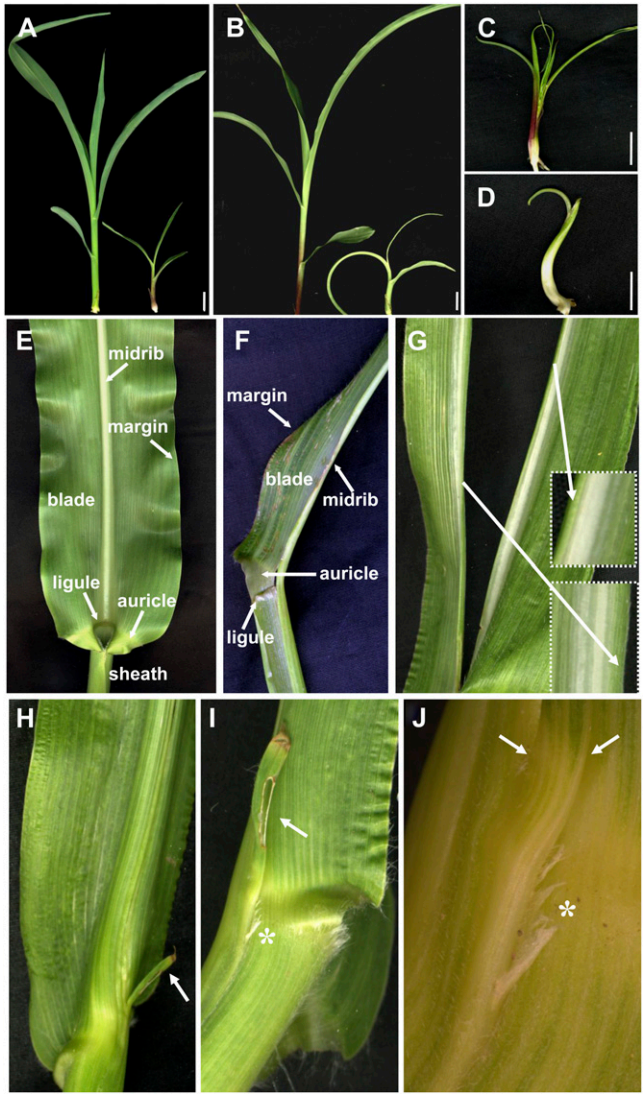

Figure 4. Mutations in *pve1* affect maize leaf patterning. Mutant pve1 seedlings are small and exhibit narrow leaves. A, Two-week-old seedling of a homozygous *pve1-R* mutant (right) and wild-type sibling (left). B, Two-week-old seedling of a homozygous *pve1-M2* mutant (right) and wild-type sibling (left). C and D, Double-mutant rgd2-R pve-M2 seedlings exhibit variable rgd2-like leaf phenotypes, ranging from small seedlings with narrow and cylindrical leaves (C) to seedlings that developed just a coleoptile and a single foliar leaf before abortion of the shoot (D). E, The maize leaf is composed of the proximal sheath and the distal blade, separated by the hinge-like auricle and an adaxial, epidermal fringe of tissue called the ligule. The leaf blade is subdivided into a central midrib, the margins, and the intervening lateral blade tissues. F, A narrow, pve1-M2 mutant half leaf. G, A pve1-R mutant split leaf that formed two midribs. Insets show close-up of the right and left leaf halves reveals that the mutant leaf has split within a narrow span of blade tissue (arrows) that formed between the two, separate midribs. H to J, An abaxially derived ectopic leaf outgrowth (arrow) from a pve1-R mutant leaf. The asterisk in I denotes an abnormal, abaxial ligule patch immediately adjacent to the ectopic leaf. J, Close-up of the ectopic abaxial leaf and the adjacent fringe of ligule tissue (asterisk); the margins of the small ectopic leaf are delineated by the arrows. Bars in A to D = 1 cm.

F2 progeny of both *pve1-R* and *pve1-M2* heterozygotes segregate small seedlings that harbor a range of noncomplementing leaf developmental phenotypes (Figs. 4 and 5), including half leaves and truncated leaf margins (Figs. 4F and 5D) as well as leaves forming two midribs (Fig. 4G) that split along a fissure plane between the two separate midribs. Equivalent phenotypes are observed in lbl1-R mutant seedling leaves, in which transacting small interfering RNA biogenesis is only moderately reduced (Timmermans et al., 1998; Nogueira et al., 2007). A striking phenotype of pve1 mutant leaves is the formation of small ectopic leaves and leaf-margin fringes (Figs. 4, H–J and 5, E and F). Ectopic outgrowths include both leaf sheath and blade tissues and are identified on adaxial as well as abaxial surfaces of pve1 mutant leaves, typically in close proximity to the midrib. Ectopic outgrowths from the abaxial leaf surface often form immediately adjacent to small patches of ectopic ligule, epidermal fringes that normally develop only on adaxial surfaces of wild-type leaves (Fig. 4, I and J). It is notable that although rgd2-R mutant leaves retain adaxial/abaxial identity, dorsiventral patterning is sometimes uncoordinated such that ectopic leaf outgrowths are also observed and are accompanied by swapping of adaxial and abaxial epidermal cell types (Henderson et al., 2005). Other pve1 mutant phenotypes include reduced SAM size (Fig. 5H) and abnormally rounded vascular bundles (Figs. 5E and 7J) characterized by a pronounced reduction in the number and size of xylem elements (Fig. 5J).

Double-mutant seedlings homozygous for both the *rgd2-R* and *pve1-M2* mutations display variable shoot and leaf morphologies (Figs. 4 and 6) that are equivalent to the range of mutant phenotypes observed in rgd2-R mutants (Fig. 1; Henderson et al., 2005). For example, some rgd2-R;pve1-M2 double mutants exhibited narrow-leaf, half-leaf, and radial-leaf phenotypes (Figs. 4C and 6B), whereas others developed just a single-mutant leaf before the abortion of the SAM arrested further shoot development (Figs. 4D and 6D). This wide range of leaf phenotypes was also observed in rgd2-R single-mutant siblings that segregated alongside rgd2-R;pve1-M2 double mutants in the F2 population, as shown in Figure 6, A and C. However, whereas the rgd2-R single mutants all had normal vascular patterning (Fig. 6, E and G), rgd2-R;pve1-M2 double mutants exhibited small, rounded vascular bundles and reduced xylem development, phenotypes that characterize pve1 solo mutants (Fig. 6, F and H). Therefore the rgd2-R;pve1-M2 double mutants display additive phenotypes, in that rgd2-R mutant leaf morphology is combined with pve1 mutant vasculature.

Altered Accumulation of Leaf Developmental Transcripts in pve1 Mutants

The accumulation of several transcripts implicated to function during dorsiventral patterning of maize leaves, including *AGO1*, the ta-siARF pathway genes *LBL1*, *TAS3A*, and *ARF3A*, and the adaxial-abaxial

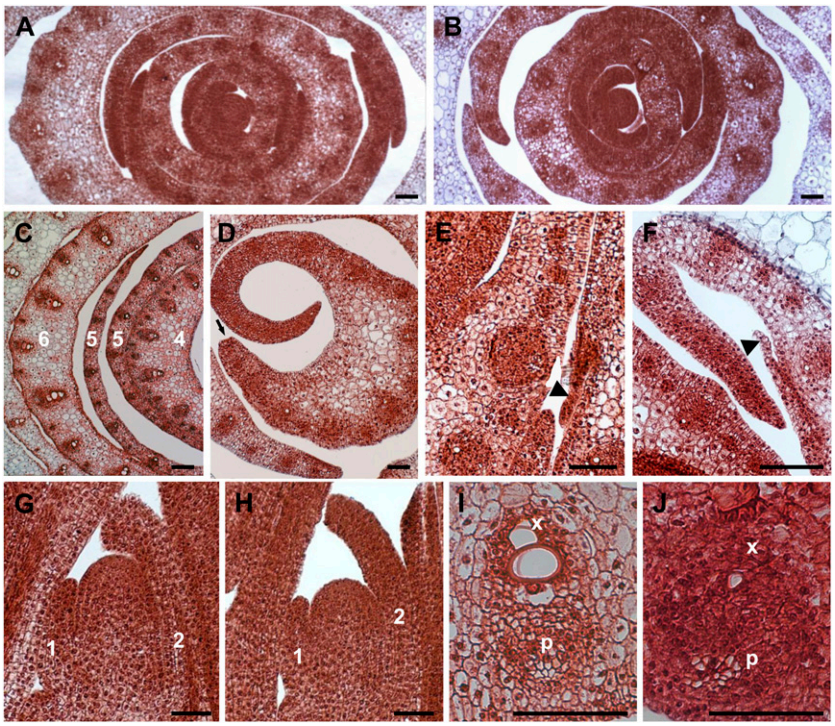

Figure 5. Microscopic pve1 mutant phenotypes. Transverse sections of wild-type (A) and pve1-M2 mutant (B) seedlings. C, Transverse section through wild-type seedling showing leaf primordia with tapered margins (5) that encircle the younger leaf (4). D, Truncated leaf of pve1-M2 mutant seedling exhibiting a half-leaf phenotype. Adaxial ectopic leaf margin outgrowths (arrows) observed in pve1-R (E) and pve-M2 (F) mutant seedlings. Longitudinal sections of the shoot apex of 14-d seedlings reveals that size of the pve1-M2 mutant SAM (H) is reduced as compared to wild-type siblings (G). I, Wild-type maize leaf vascular bundles contain large xylem (x) vessels and smaller phloem (p) vessels. J, Abnormal pve1-R mutant vascular bundles are rounded and contain fewer and smaller xylem vessels. Numbers denote leaf primordia, wherein 1 is the youngest leaf closest to the SAM. Bars = 50 μm.

identity genes *ROLLED1* (*RLD1*) and *KANADI2*, were examined via qRT-PCR analyses of pve1-R mutant seedlings to help elucidate the role of PVE1 during maize leaf development. Whereas, *RLD1*, *ARF3A*, *TAS3A*, and *LBL1* transcripts accumulate to lower levels in pve1-R mutants versus wild-type siblings, *AGO1* transcript levels are increased over 2-fold (Fig. 7). Transcript accumulation for *KANADI2* is essentially unaltered in pve1-R mutants.

In situ hybridization analyses of vascular development were performed using probes from the maize *PHB* homolog as a marker of adaxial/xylem development, and miR166 as a marker of abaxial/phloem development, as described in Juarez et al. (2004). Whereas no changes in miR166 abundance or accumulation pattern were observed in pve1-M2 seedlings as compared to wild-type siblings, accumulation of *ZmPHB* transcripts are noticeably reduced in the developing vascular bundles of pve1-M2 mutant leaves (Fig. 8).

DISCUSSION

PVE1 Functions Downstream of RGD2 during Patterning of Maize Leaves

LM microarray analyses identified *PVE1* as a gene of unknown function that is down-regulated in rgd2-R

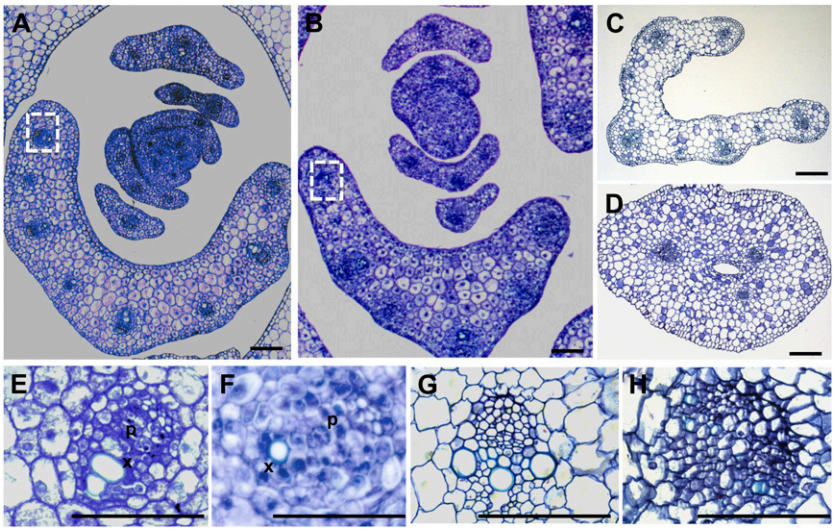

Figure 6. Vascular phenotypes of rgd2-R;pve1-M2 double mutants. Transverse sections through a *rgd2-R* homozygous mutant seedling with a moderate phenotype (A), and a sibling homozygous mutant with a more severe, single-leaf phenotype (C). Similar leaf phenotypes are observed in rgd2-R;pve1-M2 double-mutant plants, as shown in the moderately phenotypic seedling in B and the severe, single-leaf double mutant in D. Although double mutants have leaf morphology phenotypes similar to rgd2-R single mutants, rgd2-R mutants have normal vasculature (E, vascular bundle outlined in A; and G), whereas rgd2-R;pve1-M2 mutants have abnormal vasculature (F, bundle outlined in B; H) equivalent to that observed in pve1-M2 single mutants (Fig. 5). Bars = 50 μm

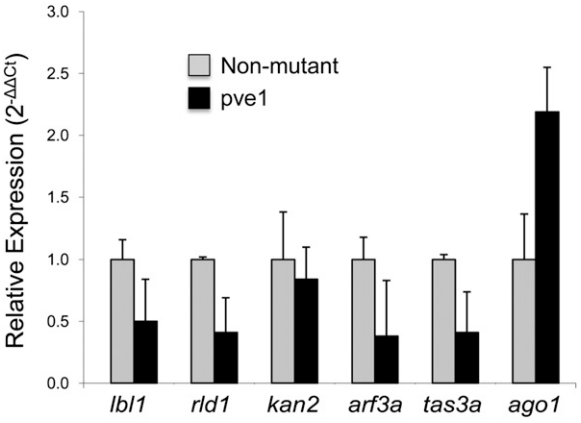

Figure 7. Transcript analyses of maize leaf developmental markers in pve1 mutant seedlings. Results of qRT-PCR analyses for genes involved in maize leaf dorsiventral patterning are presented. Three biological replicates were used for each genotype and all samples were normalized to 18s rRNA. Bars represent one SE.

mutant shoot apices (Supplemental Table S2). qRT-PCR of microdissected SAMs and of P1 to P4 leaf primordia confirmed that *PVE1* transcripts are indeed down-regulated in rgd2-R shoot apices, and analyses of lbl1-R mutant seedlings verified that both these components of the maize ta-siARF pathway promote *pve1* transcript accumulation. Notably, the *PVE1* transcript does not harbor predicted binding sites for any of the regulatory RNAs that are associated with the ta-siARF pathway, namely miR390, ta-siARF, and miR166 (Allen et al., 2005; Fahlgren et al., 2006; Nagasaki et al., 2007; Nogueira et al., 2007; Montgomery et al., 2008). We therefore speculate that *PVE1* transcription is regulated by ARF3 function, or by an additional unknown factor(s) functioning downstream of the ta-siARF pathway.

Transcripts of *PVE1* accumulate in the developing vasculature of leaf primordia, as well as in unvascularized tissues such as the leaf founder cells comprising the peripheral zone of the SAM (Fig. 2B). Within the SAM, *PVE1* accumulation precedes and appears to predict the eventual location of vascular bundles within leaf primordia. Accumulation of *PVE* transcripts is down-regulated in rgd2-R mutant apices and is delayed within the xylem vessels of developing mutant leaf primordia (Fig. 2, D–G). Vascular development is correlated with mediolateral expansion of the leaf (Dengler and Kang, 2001), such that the down-regulation of genes involved in vascular development in rgd2-R mutants is consistent with the defects in mediolateral development observed in rgd2-R leaves (Henderson et al., 2005). Although the vascular anatomy and polarity is normal in rgd2-R mutant leaves the number of vascular bundles is reduced (Fig. 2, B and E), which may result from the reduced and delayed accumulation of *PVE1* transcripts in rgd2-R mutant primordia (Fig. 2, D–G). However, *PVE1* differential expression was identified in microarray analyses of LM SAMs, tissue that is devoid of vasculature. Whereas accumulation of the maize PIN1a protein marks the vascular trace of the future midvein as early as the P0 to P1 founder cell stage of leaf initiation (Carraro et al., 2006; Gallavotti et al., 2008; Lee et al., 2009), our findings suggest that vascular patterning of lateral leaf domains also begins at the founder cell stage, well before the appearance of provascular tissues corresponding to lateral veins.

Reverse genetic analyses identified two independent transposon-insertion mutant alleles of *PVE1*, and mutant plants exhibit an array of leaf patterning phenotypes that are similar to, albeit far less severe than, those described for rgd2-R mutants (Henderson et al., 2005). These include narrow leaves and half leaves (Figs. 4 and 5). As previously described for both rgd2-R and lbl1-R mutants, pve1 mutant plants also develop ectopic leaf outgrowths that are a developmental hallmark of abnormal dorsiventral patterning (Waites and Hudson, 1995; Timmermans et al., 1998; McConnell

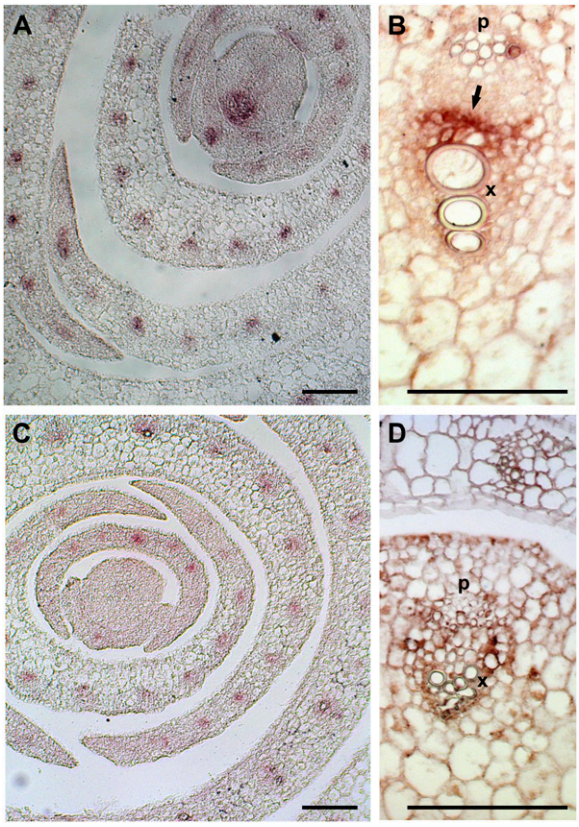

Figure 8. Altered accumulation of *ZmPHB* transcript in pve1 mutant seedlings. In situ hybridization analyses reveal transcript accumulation of the maize PHB homolog in the SAM of wild-type seedlings and in the developing vasculature of leaf primordia (A). In older (leaf 7) primordia (B), *PHB* transcript accumulation is polarized (arrow) toward the xylem (adaxial) region of the vascular bundle. C, *PHB* transcript accumulation is less abundant in pve1-M2 mutant seedlings, and is difficult to detect in the smaller vascular bundles of leaf 7 primordia. Bars = 50 μm.

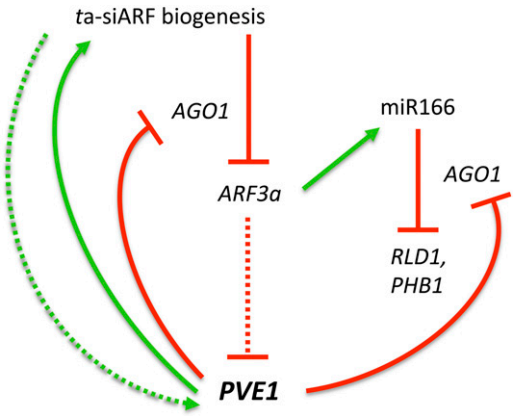

Figure 9. Model for PVE1 function in maize leaf development. PVE1 function promotes ta-siARF function and negatively regulates *AGO1*. Molecular genetic and double-mutant analyses indicate that RGD2 and PVE1 act in different pathways that interact, although it is not yet known if these interactions are direct or indirect, as indicated by the dotted lines. Details provided in the text. [See online article for color version of this figure.]

et al., 2001; Henderson et al., 2005). Consistent with the Waites and Hudson (1995) model for mediolateral leaf expansion, ectopic outgrowths on pve1 mutant leaves are associated with the abnormal juxtaposition of adaxial and abaxial tissues as indicated by the patches of adaxial ligule tissue on the abaxial leaf surface immediately adjacent to the ectopic leaf shown in Figure 4, I and J. Decreased accumulation of transcripts associated with adaxial (*RLD1*, *LBL1*, *TAS3A*) and abaxial patterning (*ARF3*) is also observed in pve1-R mutants (Fig. 7), and correlates with the observed defects in dorsiventral patterning. Unlike rgd2-R mutant leaves however, pve1 mutants have abnormal vascular development characterized by a marked reduction and delay in xylem differentiation (Fig. 5, E and J) and decreased accumulation of *ZmPHB* transcripts (Fig. 8). The question arises as to why rgd2-R mutant leaves have normal vasculature patterning in light of the fact that *PVE1* expression is down-regulated in rgd2-R mutant apices? We suggest that whereas null alleles of *pve1* develop defective vasculature, rgd2-R mutants retain approximately 20% of wild-type *PVE1* transcript levels, which is sufficient for normal vascular patterning in maize shoots.

Double-mutant analyses suggest an additive rgd2-R; pve1-M2 mutant phenotype in which severe leaf-patterning phenotypes (Fig. 4, C and D) similar to rgd2-R single mutants are found together with the severe vascular-patterning defects that characterize pve1 mutants (Fig. 6). Another interpretation is that the more severe leaf phenotypes of rgd2-R and vascular phenotypes of pve1-M2 mask the effects of the *pve1-M2* mutation in the leaf and of the *rgd2-R* mutation in the vasculature. In either scenario, these genetic data indicate that PVE1 does not function directly in the ta-siARF pathway. Our qRT-PCR analyses of pve1 mutants (Fig. 7) also suggest that PVE1 functions in a separate pathway that intersects and interacts with components of the ta-siARF pathway. Figure 9 presents a working model for PVE1 function during maize leaf patterning based upon our interpretations of the microarray data, reverse genetic analyses of pve1 mutant phenotypes, and qRT-PCR analyses of leaf developmental marker transcripts in pve1-R mutant seedlings. The reduced accumulation of both *LBL1* and *TAS3A* transcripts in pve1-R mutant seedlings suggests a feedback regulatory mechanism wherein PVE1 function promotes the ta-siARF pathway, which in turn promotes the accumulation of *PVE1* transcripts. The concomitant down-regulation of *LBL1* and up-regulation of *AGO1* in pve1-R mutant seedlings (Fig. 7) corroborates previous reports wherein LBL1 function restricts *AGO1* accumulation within the maize shoot apex (Douglas et al., 2010). Interestingly, PVE1 function also promotes the accumulation of *ARF3A* transcripts (Fig. 7). These findings suggest a complex interaction wherein PVE1 promotes ta-siARF-mediated down-regulation of *ARF3A*, and *ARF3A* accumulation correlates with down-regulation of *PVE1.* In turn, PVE1 function moderates the extent of *ARF3A* transcript down-regulation perhaps via negative regulation of *AGO1*, although it is equally unclear whether PVE1 regulates *ARF3A* via interaction with the ta-siARF or by another indirect mechanism (modeled in Fig. 9). Likewise, the reduction of *RLD1* and *ZmPHB* transcripts in pve1-R mutants (Figs. 7 and 8) may result from increased miR166 activity due to elevated levels of *AGO1.* In addition, the reduced and delayed vascular development observed in pve1 mutant seedlings may reflect the aberrant transcript accumulation of these leaf-patterning genes. Tests of the validity of this model for PVE1 function, and further resolution of the redundant complexities of ta-siARF function, will await future studies of the subcellular localization, biochemical activity, and molecular function of PVE1 and of additional downstream components of RGD2 and LBL1 function in plant shoots.

MATERIALS AND METHODS

Plant Materials

The *rgd2-R* mutation was introgressed into Mo17 for five generations. Wild-type and rgd2-R mutant maize (*Zea mays*) siblings were grown in controlled conditions with 15-h light with intensity 220 to 250 $\mu ES^{-1}\,M^{-2}$ at 25°C; and 9-h dark at 20°C. Humidity was set at 50%. Siblings were harvested for LM at 14 d after germination.

Histological Analyses

Maize seedlings harvested at 14 d after germination were fixed in formalin-acetic-alcohol, paraffin embedded, sectioned at 10 μm, and stained in either toluidine blue O or Safranin Fast Green using Johanssen's method as described (Brooks et al., 2009).

Isolation of Maize SAM RNAs

Siblings were fixed with acetone and embedded in paraffin as described (Emrich et al., 2007). The P.A.L.M. laser microbeam was used to collect SAM

cells from 10-μm sections. Each SAM typically comprised 10 to 12 longitudinal sections for LM. Six biological replicates were captured independently. Each replicate consisted of three to five whole, wild-type, or rgd2-R mutant SAMs with harvested areas varying from 0.57 to 0.95 mm^2 (Supplemental Table S1). RNA from the captured SAMs was extracted using the PicoPure RNA extraction kit (Arcturus Molecular Devices) and amplified twice (RiboAmp HS RNA amplification kit; Arcturus Molecular Devices) to yield 28 to 74 μg antisense RNA (Supplemental Table S1).

First-strand cDNA was synthesized from the amplified SAM RNA using Superscript II (Invitrogen) and purified with QIAquick PCR purification kit (QIAGEN). A total of 2.5 μg of the purified cDNA were indirectly labeled with Cy dye as described (Nakazono et al., 2003). Dye swapping was performed between biological replicates to minimize dye bias. Microarrays were hybridized as described (Nakazono et al., 2003).

Microarrays and Hybridizations

Maize SAM 1.1 (GPL3333) and SAM 3.0 (GPL3538) gene chips containing a combined total of 28,671 cDNAs were used in this experiment (Brooks et al., 2009). Detailed information about these chips is available at http://www.plantgenomics.iastate.edu/maizechip/ or MicroArray Data Interface (http://schnablelab.plantgenomics.iastate.edu:8080/madi/). The MIAME (for minimum information about a microarray experiment) guidelines utilized, hybridization protocols, and array scanning procedure were as described (Zhang et al., 2007; Brooks et al., 2009).

Microarray Data Analyses and Annotation

Each hybridized microarray gene chip was scanned with ScanArray Lite (Packard Bioscience) at 10-μm resolution. Image quantification was performed with ScanArray Express (PerkinElmer). Raw signals were first corrected by background intensity within each slide, followed by LOWESS (for locally weighted scatterplot smoothing) normalization to remove intensity-dependent dye bias (Dudoit et al., 2002). Median centering was used to normalize data across slides from each channel (Yang et al., 2002). A mixed linear model was applied to the normalized data to identify the differentially expressed genes among rgd2-R mutant and wild-type samples as described (Dudoit et al., 2002; Zhang et al., 2007). The resulting P values from the tests for SAM-type effects were converted to q values using the method of Storey and Tibshirani (2003) to estimate the false discovery rate associated with any P value threshold for significance. All microarray data are available at Gene Expression Omnibus (http://www.ncbi.nlm nih.gov/geo).

qRT-PCR and in Situ Hybridizations

Whole-plant tissue was harvested using TRIzol reagent (Invitrogen) and cDNA was synthesized using SuperScript III first-strand synthesis system (Invitrogen). SAM tissues and leaf primordia (P1–P4) tissue were harvested by LM from rgd2 mutant and wild-type siblings; cDNA was synthesized from amplified RNA as described (51). Gene-specific primers were designed (Supplemental Table S3) for use with SYBR-Green (Quanta) in qRT-PCR as described (Zhang et al., 2007). Three biological replicates were examined, and samples were normalized to *UBIQUITIN* or to 18S rRNA transcript accumulation as described using Bio-Rad iQ5 version 1.0 software (Livak and Schmittgen, 2001). All gene-specific primers utilized in this study are listed in Supplemental Table S3.

Maize 2-week-old seedlings were fixed in formalin-acetic-alcohol and processed for in situ hybridization to gene-specific probes as described (Jackson, 1991). At least six plants from each genotype (rgd2-R mutant versus wild-type sibling, and pve1-M2 versus wild-type sibling) were compared for each gene-specific probe (*PVE1*, and *ZmPHB* as described in Juarez et al., 2004) presented in the text.

Reverse Genetic Analyses

DNA samples prepared from 3,456 F2 progeny obtained by self pollination of active *Mu* transposon stocks were subjected to PCR-based screens using *pve1* gene-specific primers and a *Mu*-specific primer (AGAGAAGCCAACGCCAWCGCCTCYATTTCGTC). The gene-specific forward primer T1 (AGGGATTCATGCTACCCAGAG) was used to optimize PCR amplification conditions for two gene-specific, nested reverse primers M1 (GAGTCCGCAATCTCCATCAAC) and M2 (CCTGCAACTGAATCTGTCCAA). The first round of PCR analysis (pooled PCR) was performed with the *Mu* and M1 primers, on 96-well PCR plates with pooled four DNA samples in each well. PCR reactions were screened for specific fragments using 1% agarose gel. The corresponding DNA samples in the selected DNA sample pools were rearrayed for second round of PCR analysis using the same primer set (*Mu* and M1; deconvolution PCR). PCR reactions were then analyzed by agarose gel electrophoresis to identify individual DNA samples with specific fragments. The identified DNA samples were used for the third round of PCR amplification with the *Mu* and M2 primers (nested PCR). Meanwhile, to rule out the false-positive results derived from multiple *Mu* insertions, control reactions were performed with the *Mu* primer only. PCR reactions with specific products only from the nested PCR amplifications were sequenced to verify the *Mu* transposon insertion.

Supplemental Data

The following materials are available in the online version of this article.

Supplemental Table S1. Information for LM samples used for microarrays.

Supplemental Table S2. Microarray genes differentially expressed in the rgd2-R mutant SAM.

Supplemental Table S3. Primers utilized in this study.

Supplemental Table S4. qRT-PCR corroboration of selected rgd2-R differentially expressed genes.

ACKNOWLEDGMENTS

We thank Kate Browning, Eneda Hoxha, and Zhian Kamvar for assistance in data annotation.

Received December 19, 2011; accepted May 21, 2012; published June 5, 2012.

LITERATURE CITED

Adenot X, Elmayan T, Lauressergues D, Boutet S, Bouche N, Gasciolli V, Vaucheret H (2006) DRB4-dependant *TAS3 trans*-acting siRNAs control leaf morphology through AGO7. Curr Biol **18:** 758–762

Allen E, Xie Z, Gustafson AM, Carrington JC (2005) microRNA-directed phasing during trans-acting siRNA biogenesis in plants. Cell **121:** 207–221

Brooks LB III, Strable J, Zhang X, Ohtsu K, Zhou R, Sarkar A, Hargreaves S, Elshire RJ, Eudy D, Pawlowska T, et al (2009) Microdissection of shoot meristem functional domains. PLoS Genet **5:** e1000476

Carraro N, Forestan C, Canova S, Traas J, Varotto S (2006) *ZmPIN1a* and *ZmPIN1b* encode two novel putative candidates for polar auxin transport and plant architecture determination of maize. Plant Physiol **142:** 254–264

Dengler N, Kang J (2001) Vascular patterning and leaf shape. Curr Opin Plant Biol **4:** 50–56

Douglas RN, Wiley D, Sarkar A, Springer N, Timmermans MCP, Scanlon MJ (2010) *ragged seedling2* encodes an ARGONAUTE7-like protein required for mediolateral expansion, but not dorsiventrality, of maize leaves. Plant Cell **22:** 1441–1451

Dudoit S, Yang YH, Callow MJ, Speed TP (2002) Statistical methods for identifying genes with differential expression in replicated cDNA microarray experiments. Statist Sinica **12:** 111–139

Emrich SJ, Barbazuk WB, Li L, Schnable PS (2007) Gene discovery and annotation using LCM-454 transcriptome sequencing. Genome Res **17:** 69–73

Fahlgren N, Montgomery TA, Howell MD, Allen E, Dvorak SK, Alexander AL, Carrington JC (2006) Regulation of *AUXIN RESPONSE FACTOR3* by *TAS3* ta-siRNA affects developmental timing and patterning in *Arabidopsis.* Curr Biol **16:** 939–944

Gallavotti A, Yang Y, Schmidt RJ, Jackson D (2008) The relationship between auxin transport and maize branching. Plant Physiol **147:** 1913–1923

Henderson DC, Muehlbauer GJ, Scanlon MJ (2005) Radial leaves of the maize mutant *ragged seedling2* retain dorsiventral anatomy. Dev Biol **282:** 455–466

Hunter C, Willmann MR, Wu G, Yoshikawa M, de la Luz Gutiérrez-Nava M, Poethig SR (2006) Trans-acting siRNA-mediated repression of

ETTIN and ARF4 regulates heteroblasty in *Arabidopsis*. Development **133:** 2973–2981

Jackson D (1991). In situ hybridization in plants. *In* DJ Bowles, SJ Gurr, M McPherson, eds, Molecular Plant Pathology: A Practical Approach. Oxford University Press, Oxford, pp 163–174

Jackson D, Veit B, Hake S (1994) Expression of the maize *KNOTTED-1* related homeobox genes in the shoot apical meristem predicts patterns of morphogenesis in the vegetative shoot. Development **120:** 405–413

Juarez MT, Kui JS, Thomas J, Heller BA, Timmermans MCP (2004) microRNA-mediated repression of rolled leaf1 specifies maize leaf polarity. Nature **428:** 84–88

Lee BH, Johnston R, Yang Y, Gallavotti A, Kojima M, Travençolo BA, Costa LdaF, Sakakibara H, Jackson D (2009) Studies of aberrant phyllotaxy1 mutants of maize indicate complex interactions between auxin and cytokinin signaling in the shoot apical meristem. Plant Physiol **150:** 205–216

Livak KJ, Schmittgen TD (2001) Analysis of relative gene expression data using real-time quantitative PCR and the 2(-Delta Delta C(T)) method. Methods **25:** 402–408

McConnell JR, Barton MK (1998) Leaf polarity and meristem formation in Arabidopsis. Development **125:** 2935–2942

McConnell JR, Emery J, Eshed Y, Bao N, Bowman J, Barton MK (2001) Role of PHABULOSA and PHAVOLUTA in determining radial patterning in shoots. Nature **411:** 709–713

Montgomery TA, Howell MD, Cuperus JT, Li D, Hansen JE, Alexander AL, Chapman EJ, Fahlgren N, Allen E, Carrington JC (2008) Specificity of ARGONAUTE7-miR390 interaction and dual functionality in TAS3 trans-acting siRNA formation. Cell **133:** 128–141

Nagasaki H, Itoh J, Hayashi K, Hibara K, Satoh-Nagasawa N, Nosaka M, Mukouhata M, Ashikari M, Kitano H, Matsuoka M, et al (2007) The small interfering RNA production pathway is required for shoot meristem initiation in rice. Proc Natl Acad Sci USA **104:** 14867–14871

Nakazono M, Qiu F, Borsuk LA, Schnable PS (2003) Laser-capture microdissection, a tool for the global analysis of gene expression in specific plant cell types: identification of genes expressed differentially in epidermal cells or vascular tissues of maize. Plant Cell **15:** 583–596

Nogueira FT, Chitwood DH, Madi S, Ohtsu K, Schnable PS, Scanlon MJ, Timmermans MC (2009) Regulation of small RNA accumulation in the maize shoot apex. PLoS Genet **5:** e1000320

Peragine A, Yoshikawa M, Wu G, Albrecht HL, Poethig RS (2004) SGS3 and SGS2/SDE1/RDR6 are required for juvenile development and the production of trans-acting siRNAs in *Arabidopsis*. Genes Dev **18:** 2368–2379

Poethig RS (1984). Cellular parameters of leaf morphogenesis in maize and tobacco. *In* RA White, WC Dickinson, eds, Contemporary Problems of Plant Anatomy. Academic Press, New York, pp 235–238

Poethig RS, Szymkowiak EJ (1995) Clonal analysis of leaf development in maize. Maydica **40:** 67–76

Smith LG, Greene B, Veit B, Hake S (1992) A dominant mutation in the maize homeobox gene, *Knotted-1*, causes its ectopic expression in leaf cells with altered fates. Development **116:** 21–30

Storey JD, Tibshirani R (2003) Statistical significance for genomewide studies. Proc Natl Acad Sci USA **100:** 9440–9445

Timmermans MC, Schultes NP, Jankovsky JP, Nelson T (1998) Leafbladeless1 is required for dorsoventrality of lateral organs in maize. Development **125:** 2813–2823

Waites R, Hudson A (1995) *phantastica*: a gene required for dorsoventrality of leaves in *Antirrhinum majus*. Development **121:** 2143–2154

Yoshikawa M, Peragine A, Park MY, Poethig RS (2005) A pathway for the biogenesis of *trans*-acting siRNAs in *Arabidopsis*. Genes Dev **19:** 2164–2175

Zhang X, Madi S, Borsuk L, Nettleton D, Elshire RJ, Buckner B, Janick-Buckner D, Beck J, Timmermans M, Schnable PS, et al (2007) Laser microdissection of narrow sheath mutant maize uncovers novel gene expression in the shoot apical meristem. PLoS Genet **3:** e101